ELSEVIER

Journal of Power Sources 107 (2002) 74–79

JOURNAL OF POWER SOURCES

www.elsevier.com/locate/jpowsour

Evaluation of discharge and cycling properties of skutterudite-type $Co_{1-2y}Fe_yNi_ySb_3$ compounds in lithium cells

L. Monconduit[a], J.C. Jumas[a], R. Alcántara[b], J.L. Tirado[b], C. Pérez Vicente[b,*]

[a]*Laboratoire des Agrégats Moléculaires et Matériaux Inorganiques UPR ESA 5072, Université Montpellier II, Place Eugène Bataillon, 34095 Montpellier, France*

[b]*Laboratorio de Química Inorgánica, Edificio C3, Planta 1, Campus de Rabanales, Universidad de Córdoba, 14071 Córdoba, Spain*

Received 26 June 2001; received in revised form 10 October 2001; accepted 20 October 2001

Abstract

The preparation, structural characterization and study of the electrochemical behavior in lithium cells of $Co_{1-2y}Fe_yNi_ySb_3$ ($0.125 < y \leq 0.5$) compounds is described. The refinement of X-ray diffraction (XRD) patterns evidenced the skutterudite-type structure for all compositions, with an increasing partial filling of 2a sites. The first discharge of lithium anode cells shows two plateaus. The plateau at higher potential, which occurs at ca. 0.8 V and extends from ca. 150 to 250 Ah/kg depending on "y", is mainly assigned to side reactions of lithium with the electrolyte, as confirmed by ^{7}Li NMR. The second plateau occurs at 0.5–0.6 V and is assigned to Li–Sb alloys formation. The charge of the cell shows that only the second step is reversible. Further discharge/charge cycles present a plateau at 0.8 V in the discharge and at 1.05 V in the charge, which agree well with the Li–Sb alloying/de-alloying process. Extended cycling results on a loss of capacity, to stabilize over 100 Ah/kg after 20 cycles.

Keywords: Skutterudite; Lithium battery; Lithium antimony alloy

1. Introduction

Although the use of Li-Metal alloys as electrode material is well known long time ago, the interest in lithium alloys has been renewed from the announcement by FujiPhoto Film Co. [1] on the performances of tin-based oxy-glasses. This interest concerns not only tin-based compounds, but also other elements which are not as "environmental friendly" as tin. Thus, intermetallic antimony-based compounds have been studied. Weppner and Huggings reported the coulometric titration of Sb with Li at 400 °C in a molten salt electrolyte [2]. Later, the potential versus composition curves of Sb alloys at 25 °C was reported, characterized by a plateau at 0.95 V assigned to the formation of Li_3Sb [3]. More recently, other Sb-based compounds have been studied, such as SnSb [4–6], $CrSb_2$ [7], InSn [8], and skutterudite-type $CoSb_3$ [9].

The structure of skutterudite is related to that of perovskite ABX_3 (space group $Pm\bar{3}m$), by tilting each octahedron through a fixed angle ϕ, resulting in two different types of A atoms. The new unit cell has the composition $A'_2\,A''_6B_8Sb_{24}$. If vacancies are present in both A′ and A″ sites, the typical skutterudite-type structure is obtained, as Fig. 1A and B illustrate. On the contrary, if one of the two sets of A sites is occupied (A′), the so-called filled skutterudite is obtained (Fig. 1C and D). From the point of view of their application, these Sb-based compounds show potential application as thermoelectric ($MFe_{4-x}Co_xSb_{12}$, M = Ce, La, $0 < x < 4$) [10] and as precursor of active anodic material ($CoSb_3$) [9]. Thus, in this work we evaluate the discharge properties and cycling behavior of $Co_{1-2y}Fe_yNi_ySb_3$ ($y = 0.125$, 0.25, 0.375, 0.5) in lithium cells, where the substitution by Fe + Ni is chosen for being isolelectronic to Co, to study the influence of the transition metal in the electrochemical behavior. Additionally, due to the relatively high price of Co, its partial substitution by other cheaper transition metals (as Fe and Ni) has also been studied in other systems, such as in $LiCoO_2$.

2. Experimental

Compounds with nominal composition $Co_{1-2y}Fe_yNi_ySb_3$ ($y = 0.125$, 0.25, 0.375, 0.5) were prepared in the following way: stoichiometric quantities of the powdered elements (commercial Aldrich antimony, purity 99.5%; cobalt, purity 99.995%; iron, purity 99.99%; and nickel, purity 99.999%)

* Corresponding author. Fax: +34-957-218606.
E-mail address: iq3pevic@uco.es (C. Pérez Vicente).

0378-7753/02/$ – see front matter
PII: S0378-7753(01)00988-0

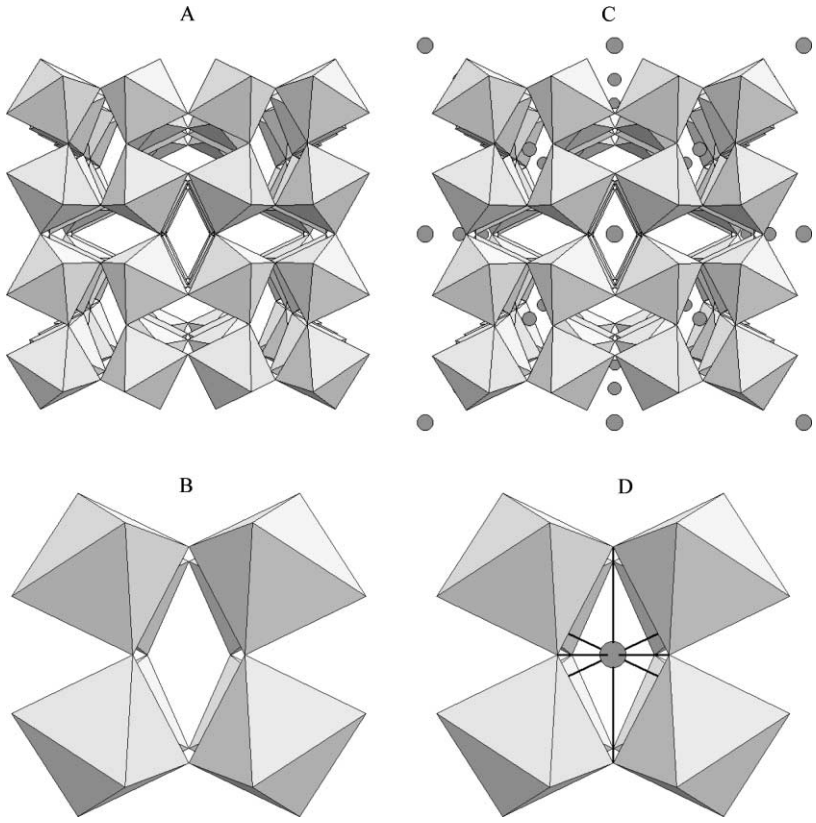

Fig. 1. (A) Projection of the skutterudite structure along [0 0 1] direction, showing [$CoSb_6$] octaedra; (B) zoom showing the octahedral coordination around an empty site 2a (0,0,0); (C) projection of a filled skutterudite, showing where the filling atoms are inserted; (D) zoom showing in detail the coordination of the filling atoms in the site 2a.

were intimately mixed and placed in evacuated, sealed quartz tubes. The mixtures were heated at 50 °C/h up to 750 °C for 1 week, then crushed, re-annealed for a further week at 700 °C and finally cooled to room temperature at 10 °C/h. The materials were carefully handled in an argon-filled glove box throughout the all synthesis process to prevent unexpected contamination. X-ray diffraction (XRD) patterns were recorded on a Philips diffractometer, using Cu Kα radiation with graphite monochromator.

^{7}Li magic-angle spin (MAS) NMR spectra were recorded at room temperature on a Bruker ACP-400 spectrometer working at 155.52 MHz resonance frequency and at ca. 4.5 kHz spinning rate. The lithium reference was a 1 M LiCl aqueous solution.

Two-electrode Swagelok cells of the type Li/$LiPF_6$(EC:-DEC)/$Co_{1-2y}Fe_yNi_ySb_3$ were used in the electrochemical measurements. The electrodes were prepared as 7 mm diameter pellets by pressing a mixture of 60% of the active compound (typically 8–10 mg), 10% of PTFE and 30% of carbon-black, on a stainless steel grid. Lithium electrodes consist on a clean 7 mm diameter lithium metal disc. The electrolyte was a commercial Merck solution of 1 M $LiPF_6$ in a 1:1 mixture of ethylene carbonate (EC) and diethylene carbonate (DEC), supported by porous glass–paper disc (Whatman). Electrochemical studies were carried out by using a MacPile II system. Galvanostatic experiments were performed at *C*/4 rate ($C = 1$ Li mol^{-1} h^{-1}). Potentiostatic experiments were performed in steps of 20 mV and relaxation time of 1 h per step. The discharge/charge experiments were carried out under galvanostatic conditions and limited to the 0–1.5 V interval.

3. Results and discussion

3.1. Structural characterization

The phase-purity of the pristine compounds $Co_{1-2y}Fe_y$-Ni_ySb_3 ($0.125 < y \leq 0.5$) was checked by XRD. Impurities of metallic antimony (2–9%) were detected in all cases. The experimental XRD patterns were fitted by the Rietveld method using the $Im\bar{3}$ cubic space group (no. 204). Initially, the following atomic distribution was assumed: Sb in site 24g (0, *y*, *z*) ($y = 0.344$, $z = 0.160$) and Co, Ni, Fe in site 8c (1/4, 1/4, 1/4) [11]. Due to the detected Sb impurities, the site occupation factor of 24g site was refined. Because of the relatively high values obtained for the reliability factors, Ni, Fe and Co were also allowed to occupy the 2a site, to give partially filled skutterudite-type structures, as Fig. 1 shows. Fig. 2 includes the experimental and refined XRD patterns, as well as their difference, corresponding to the sample $Fe_{0.5}Ni_{0.5}Sb_3$. Similar results were obtained for other samples.

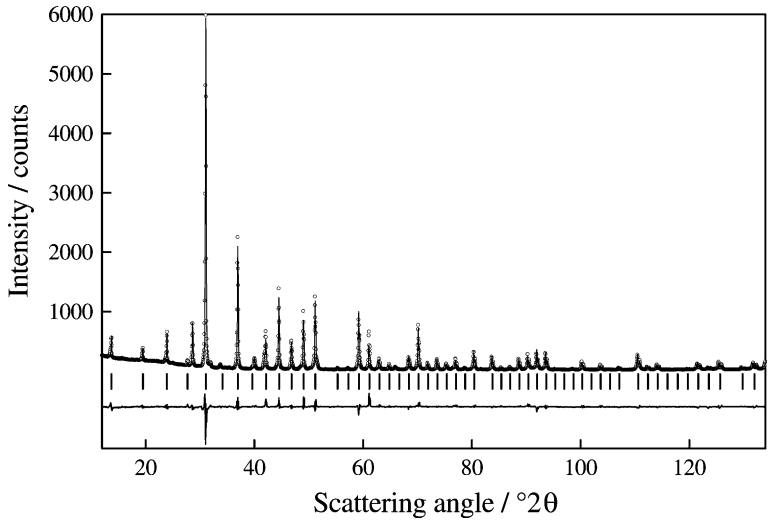

Fig. 2. Experimental (dotted) and refined (full line) XRD pattern of $Fe_{0.5}Ni_{0.5}Sb_3$. The position of the reflections are indicated by vertical bars. The difference between experimental and refined patterns is shown at the bottom.

Table 1 resumes the main results of these refinements. The evolution of the lattice constant was linear with Co content, although at low Co concentration XRDs indicate an increasing filling of the skutterudite structure in 2a site.

To complete the study of this series of compounds, we also tried to synthesize other mixed compounds such as $Ni_zCo_{1-z}Sb_3$ and $Fe_zCo_{1-z}Sb_3$, but a mixture of several phases were obtained (Sb, $FeSb_2$, $CoSb_2$, $CoSb_3$, ...), as described elsewhere [12].

3.2. Electrochemical behavior

First discharge curves of lithium anode cells using $Co_{1-2y}Fe_yNi_ySb_3$ as active cathode material are shown in Fig. 3. They are characterized by the presence of two plateaus. The voltage of the second plateau, between 0.55 and 0.6 V, agrees well with the formation of lithium antimony alloys. The formation of 3 mol Li_3Sb from $Co_{1-2y}Fe_yNi_ySb_3$ implies a theoretical consumption of 9 F/mol, which agrees fairly well with the observed extension of this plateau.

The first plateau ends at ca. 160 Ah/kg for $y = 0.5$. A decrease in y results in an increase of the capacity value at the end of this first step, as the inset in Fig. 3 clearly shows. A similar plateau was observed in the case of $SnSb_x$, related with the formation of Li_3Sb and Sn. The volume expansion was buffered by the presence of two different phases in the $SnSb_x$ alloy, which reacts at different potential [4,13]. This

Table 1
Summary of crystallographic data and refined parameters of $Co_{1-2y}Fe_yNi_ySb_3$[a]

	y in $Co_{1-2y}Fe_yNi_ySb_3$			
	$y = 0.125$	$y = 0.25$	$y = 0.375$	$y = 0.5$
Crystal system	Cubic			
Space group	$Im\bar{3}$ (204)			
a (Å)	9.0494 (1)	9.0626 (1)	9.0739 (1)	9.08734 (9)
V (Å)	741.08 (1)	744.31 (1)	747.12 (1)	750.43 (1)
Site 2a (0,0,0)	Atoms: Fe + Ni + Co			
Occupation factor (%)	14 (2)	18 (2)	25 (2)	48 (4)
Site 8c (1/4, 14, 1/4)	Atoms: Fe + Ni + Co			
Occupation factor(%)	100			
Site 24g (0, y, z)	Atom: Sb			
Y	0.3354 (2)	0.3344 (1)	0.3350 (1)	0.3360 (2)
Z	0.1579 (2)	0.1558 (1)	0.1581 (2)	0.1560 (2)
Occupation factor (%)	95 (1)	95 (1)	98 (1)	95 (1)
Impurities	Sb	Sb	Sb	Sb, $FeNiSb_6$
R_{wp}[a] (%)	11.25	11.70	10.30	10.66
Goodness of fit	1.40	1.58	1.44	1.02

[a] $R_{wp}(\%) = 100\left(\frac{\sum w_i(y_{i,e}-y_{i,c})^2}{\sum w_i y_{i,e}^2}\right)$.

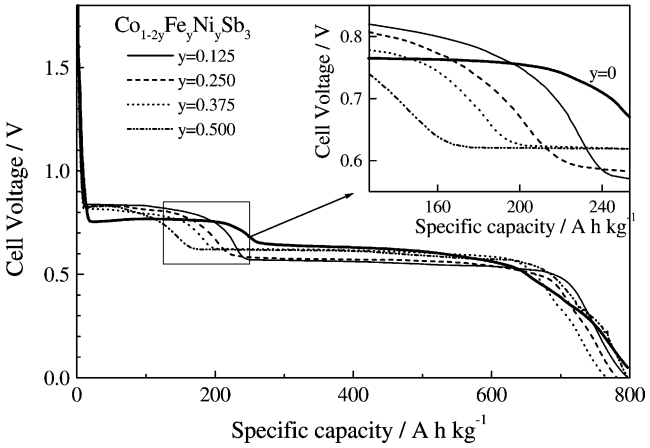

Fig. 3. Discharge curves using $Co_{1-2y}Fe_yNi_ySb_3$ as cathode material in lithium cells. Data for $CoSb_3$ ($x = 0$) showed in the inset are taken from [9].

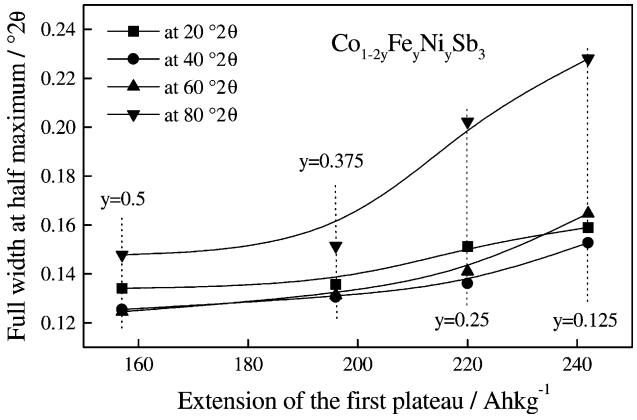

Fig. 4. Evolution of the full width at half maximum (FWHM) of Bragg reflections for the different samples as a function of the extension of the first plateau at selected scattering angles.

lithium insertion was described for InSb [14], with a volume cell expansion of ca 4.4%. InSb has a sphalerite-type structure, which is a more compact structure, thus Li insertion displaces In from the structure, which is accompanied by changes in the volume cell. Since skutterudite has a relatively open structure, lithium insertion could takes place without cell expansion, and the possibility of Li insertion cannot be directly inferred from XRD data, as exposed above.

A similar Li insertion could be assumed in $Co_{1-2y}Fe_yNi_ySb_3$ compounds at the beginning of the discharge, locating Li atoms in the tunnels present in the structure. A previous study on $CoSb_3$ [9] showed a decrease in crystallinity of the product during this first plateau, but being reflection always visible. No increase of the volume cell was detected. Anyway, in the coordination polyhedron of the vacancies represented in Fig. 1 C and D, the distance between two opposite corners is ca. 6.7 Å, while the path to move from one to another coordination polyhedron is limited by a pseudo-rhombus, which diagonals are 2.86 and 6.07 Å. This size of tunnel can allow insertion and diffusion of Li atoms within the structure without expansion. Assuming the complete filling of these vacancies, the nominal composition will be $A_{0.25}MSb_3$ (M = Fe, Co, Ni), where A refers to M initially present in 2a sites in the pristine compound plus the possible inserted lithium during electrochemical experiment. Taking into account that the pristine compounds are partially filled (see occupation factors of the 2a site in Table 1), the maximum inserted lithium amount that can be accommodated in the vacancies vary from 0.13 to 0.21 Li per $Co_{1-2y}Fe_yNi_ySb_3$ formula, depending on the y value. Even if an almost linear evolution of the extension of the plateau with the occupancy of the site 2a is observed, these values are far from the experimental extension of the first plateau. Thus, a side reaction has to be accepted.

An additional mechanism has been proposed to explain this divergence: the formation of a solid electrolyte interface (SEI) layer as a result of the reaction of lithium with the electrolyte at the surface of the metal particles. These two mechanism (Li insertion and SEI) have also been proposed in carbon-based electrodes in a similar voltage window. Dey [15] proposed the formation of Li_2CO_3. Also the occurrence of $ROCO_2Li$ has been described [16] as a result of solvent reactions at the surface of carbonaceous anode. This effect has been previously described for the skutterudite-type $CoSb_3$ [9]. This reaction is expected to be affected by the effective surface of the compound, i.e. by the particle size, which can be related with the width of Bragg reflections in XRD patterns. Fig. 4 plots the evolution of the full width at half maximum (FWHM) of Bragg reflections for the different samples as a function of the extension of the first plateau at selected scattering angles. The average grain size of the materials, calculated from the Scherrer formula, are 100, 113, 128 and 132 Å, for $y = 0.125$, 0.25, 0.375 and 0.5, respectively. It evidences that the lower values of grain size, the larger extension of the plateau. From the above discussion, it can be inferred that the first step of the discharge could involve the formation of a SEI layer film as a result of the reaction of lithium with the electrolyte at the surface of the metal particles. However, as the extension of the irreversible plateau is notably high while the reversible capacity is close to the theoretical capacity for Li_3Sb formation, the assignment of the first step to electrolyte decomposition may involve not only the formation of the SEI layer, but also additional reactions with the electrolyte. Particularly if the stability of the SEI layer is not high, as recently proposed in SnSb by Wachtler et al. [6].

Fig. 5 shows the ^7Li MAS NMR spectra of the sample $Fe_{0.5}Ni_{0.5}Sb_3$ at different depth of discharge. The refined parameters are included in Table 2. At 0.5 and 1.0 Li per $Fe_{0.5}Ni_{0.5}Sb_3$ formula (ca. 31.7 and 63.4 Ah/kg, respectively Fig. 5A) only a large signal centered at −0.5 and −0.1 ppm is present for 0.5 and 1.0 Li, respectively. This signal is ascribable to ionic forms of lithium, such as lithium carbonate and $ROCO_2Li$ species, which are expected to be formed during the generation of the SEI layer. As the observed

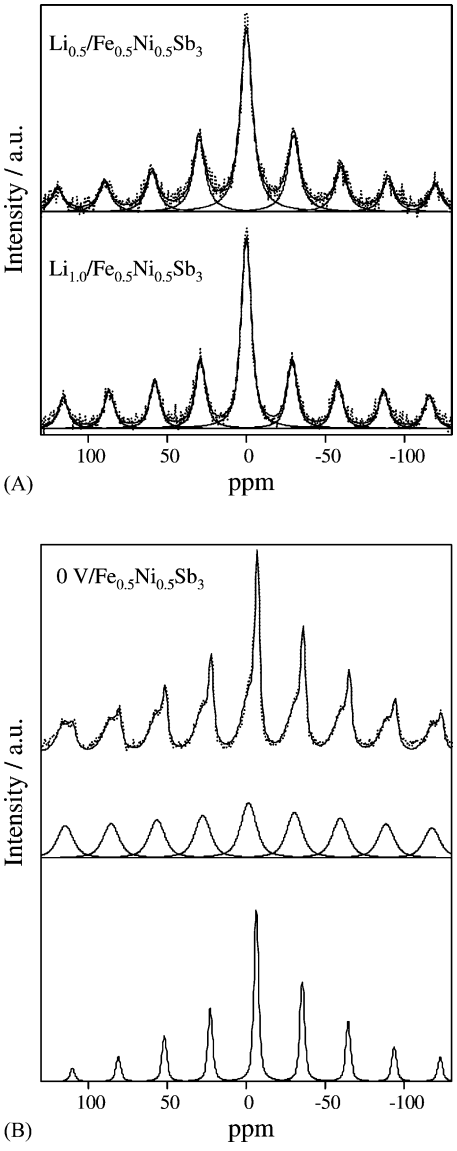

Fig. 5. (A) ^{7}Li MAS NMR of lithiated $Fe_{0.5}Ni_{0.5}Sb_3$ at 0.5 (top) and 1.0 (bottom) Li per formula; (B) ^{7}Li MAS NMR of lithiated $Fe_{0.5}Ni_{0.5}Sb_3$ at the end of the first discharge.

signal is the envelope of the different lithium species, a broad profile is visible. Thus, an hypothetical ionic lithium insertion during the first steps of the discharge could not be evidenced.

Table 2
Chemical shift and width of the refined signal corresponding to the experimental ^{7}Li MAS NMR spectra in Fig. 5

Discharged at	Chemical shift (ppm)	Full width at half maximum (ppm)	Attribution
0.5 Li = 31.7 Ah (kg)	−0.49	8.97	SEI
1.0 Li = 63.4 Ah (kg)	−0.11	7.67	SEI
Total discharge (0 V)			
	−1.62	11.87	SEI
	−6.69	3.53	Li–Sb alloy

The ^{7}Li MAS NMR spectrum shown in Fig. 5B corresponds to sample $Fe_{0.5}Ni_{0.5}Sb_3$ at the end of the discharge. It shows two signals centered at −1.6 and −6.7 ppm. The first one, larger and lower in intensity, can be assigned to the SEI layer, as in the above cases. The second, narrower and more intense, can be ascribable to Li–Sb alloy. The −6.7 ppm chemical shift agrees with covalently bonded lithium, typically ranging from +5 to −10 ppm, relative to aqueous LiCl [17]. This results differs from that observed in Li–Sn alloys. Thus, for example, the Li_7Sn_3 alloy show a main signal centered at 17 ppm, and a smaller peak at ca. 43 ppm [18], where the positive values of chemical shift arise from Knight shift interactions. For $Li_{22}Sn_5$ alloy the major component is centered at 69 ppm, evidencing a stronger Knight shift. On the contrary, when SnO is used as cathode vs. lithium in Li-cells, and discharged to reach Li/SnO = 6.4, which corresponds to the theoretical formation of $Li_{22}Sn_4$, the main component appears at 8 ppm. It was difficult to assign this component to a particular local environment of Li in the alloy, which reflects the low crystallinity and lack of conductivity of the lithiated product as compared with chemically prepared Li–Sn alloys [18]. In this way, a similar effect can undergo during the lithiation of $Fe_{0.5}Ni_{0.5}Sb_3$, to yield a Li–Sb alloys of low crystallinity and low conductivity, resulting on the absence of the Knight shift and thus on negative chemical shift.

Fig. 6 shows the results of the potentiostatic discharge of selected samples. Similar results were obtained for all the series. The first potentiostatic discharge shows two peaks ascribable to the above described plateaus. Only one plateau was observed in the galvanostatic charge curve (a peak in

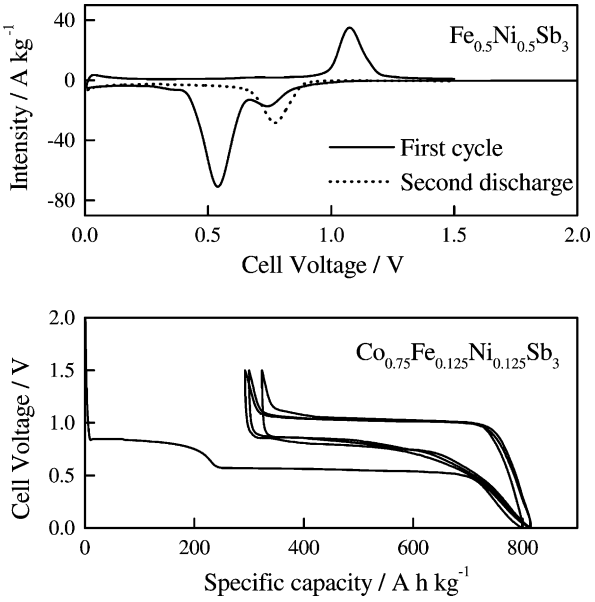

Fig. 6. Top: potentiostatic discharge/charge curve using $Fe_{0.5}Ni_{0.5}Sb_3$ as active electrode material in lithium cells. Bottom: potentiostatic discharge/charge curve using $Co_{0.75}Fe_{0.125}Ni_{0.125}Sb_3$ as active electrode material in lithium cells.

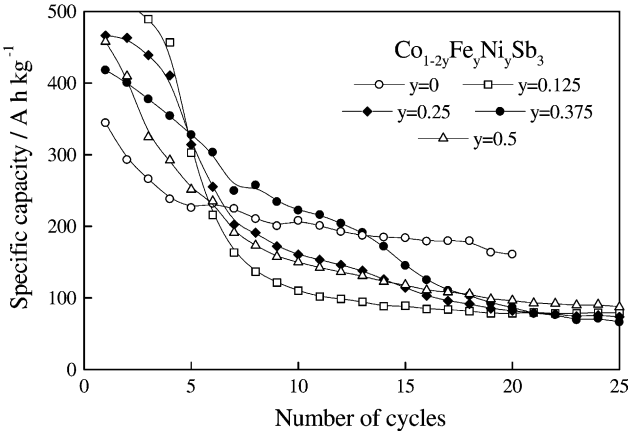

Fig. 7. Evolution of the capacity in charge as a function of the number of cycles. Data for $CoSb_3$ are taken from [9].

the potentiotatic discharge curve) at ca. 1.05 V. Further discharges did not show the first step of the discharge. Only a plateau appears at ca. 0.8 V. These charge/discharge plateaus agree well with those described when pure Sb is used as active electrode material [9]. This result confirms that the cyclability of this series of compounds is based in the Li–Sb alloying/de-alloying, and that the first step observed in the first discharge is not reversible, as expected.

Finally, the evolution of the capacity as a function of the number of discharge/charge cycles is represented in Fig. 7. The initial capacities are over 400–500 Ah/kg, but a strong loss of capacity took place during the first cycles, to be finally stabilized at ca. 100 Ah/kg, except for $CoSb_3$ whose capacity was close to 200 Ah/kg [9]. Although the substitution of Co by Ni and Fe could be interesting from an economic point of view, and the theoretical capacity of the Li–Sb alloying could also make them interesting compounds as precursors for active negative electrode in rocking-chair batteries, a hard work has to be developed concerning the electrode design to practical applications.

Acknowledgements

The authors are grateful to CICYT for financial support (contracts MAT99-0741 and HF1999-0002).

References

[1] Y. Idota, T. Kubota, A. Matsufuji, Y. Maekawa, T. Miyasaka, Science 276 (1997) 1395.
[2] W. Weppner, R.A. Huggins, J. Electrochem. Soc. 125 (1978) 7.
[3] J. Yang, I.D. Raistrick, R.A. Huggins, J. Electrochem. Soc. 133 (1986) 457.
[4] J.O. Besenhard, J. Yang, J.M. Winter, J. Power Sources 68 (1997) 87.
[5] J. Yang, M. Wachtler, J.O. Besenhard, M. Winter, Electrochem. Soc. Lett. 2 (1999) 161.
[6] M. Wachtler, M. Winter, J.O. Besenhard, J. Power Sources 94 (2001) 189.
[7] F.J. Fernández Madrigal, P. Lavela, C. Pérez Vicente, J.L. Tirado, J. Electroanal. Chem. 501 (2001) 205.
[8] C.S. Johson, J.T. Vaughley, M.M. Thackeray, T. Sarakonsi, S.A. Hackney, L. Fransson, K. Edström, J.O. Thomas, Electrochem. Commun. 2 (2000) 595.
[9] R. Alcántara, F.J. Fernández Madrigal, P. Lavela, J.L. Tirado, J.C. Jumas, J. Olivier-Fourcade, J. Mater. Chem. 9 (1999) 2517.
[10] B.C. Sales, D. Mandrus, R.K. Williams, Science 272 (1996) 1325.
[11] A. Kjekshus, D.G. Nicholson, T. Rakke, Acta Chem. Scand. 27 (1973) 1315.
[12] L.J. Zhang, X.B. Zhao, X.B. Jiang, C.P. Ly, G.S. Cao, J. Power Sources 94 (2001) 92.
[13] J. Yang, Y. Takeda, Q. Li, N. Imanishi, O. Yamamoto, J. Power Sources 90 (2000) 64.
[14] G. Herren, N.E. Walsöe, Solid State Ionics 47 (1991) 57.
[15] A.N. Dey, Thin Solid Films 43 (1977) 131.
[16] D. Aurbach, Y. Ein-Eli, J. Electrochem. Soc. 142 (1995) 1746.
[17] J.W. Akitt, in: J. Mason (Ed.), Multinuclear NMR, Plenum Press, New York, 1987, p. 192.
[18] Y. Wang, J. Sakamoto, C.K. Huang, S. Surampuri, S.G. Greenbaum, Solid State Ionics 110 (1998) 167.